PAPER

Check for updates

Enhanced photocatalytic performance of tetraphenylethylene-based porous aromatic frameworks by bandgap adjustment for the synthesis of benzimidazoles†

He Wang,[a] Xinmeng Xu,[a] Linzhu Cao,[a] Zhenwei Zhang,[b] Jiali Li,[b] Xiaoming Liu, [iD][b] Xin Tao [iD] *[a] and Guangshan Zhu [iD][a]

Porous aromatic frameworks (PAFs) as visible-light active and reusable photocatalysts provide a green and sustainable alternative to conventional metal-based photocatalysts. In this study, we design and synthesize three novel photoactive tetraphenylethylene (TPE) based PAF photocatalysts (TPE-PAFs) linked with thiophene units in an alternating donor (D)−acceptor (A) fashion. Photoelectrochemical measurements show that the introduction of different thiophene units can effectively regulate the optical band gap and energy level, which may further determine their photocatalytic performance. As a result, TPE-PAFs achieve excellent yields (up to 99%), broad substrate scope and high recyclability (up to 10 cycles) for the photosynthesis of benzimidazoles. The photocatalytic reaction is successfully monitored using *in situ* IR spectra. This work provides a feasible approach for designing PAFs with high photocatalytic activity and broadens the application of PAFs for photocatalytic organic transformations.

Broader context

Creating effective and eco-friendly approaches to promote the utilization of clean energy and to combat environmental pollution is of great significance. Visible-light-driven strategies, which convert clean solar energy to chemicals, have been recognized as a powerful synthetic platform to achieve chemical transformations. Specifically, photocatalysis has been successfully applied to the synthesis of pharmaceutically and biologically relevant molecules. Seeking for durable, cost-effective, metal-free, non-toxic, and recyclable heterogeneous photocatalysts remains a challenge. Porous aromatic frameworks (PAFs) are organic porous materials formed by polymerization of aromatic units. PAFs exhibit high stability under harsh chemical treatments, due to their strong carbon−carbon bonding character. Furthermore, the local structure of PAFs becomes tunable through framework design and organic synthesis. These unique features render PAFs a feasible and promising platform for constructing efficient photocatalysts. In this study, the combination of tetraphenylethylene (TPE) fragments with different thiophene units in an alternating donor (D)–acceptor (A) fashion affords novel TPE-PAF photocatalysts, with adjustable optical band gaps and energy levels. It is found that TPE-PAFs can achieve excellent yields, broad substrate scope and good recyclability for the photosynthesis of benzimidazoles, which are key building blocks for several heterocyclic scaffolds widely found in drugs and functional materials.

Introduction

Visible-light-driven photocatalytic reactions have emerged as environmentally friendly and sustainable approaches for crafting intricate chemical compounds.[1–4] High-performance, non-polluting, and sustainable photocatalysts are of great interest.[5,6] Currently, organic dyes find extensive utility in photocatalytic reactions due to their commendable light absorption capability and abundant redox potentials in the excited states.[7,8] Metal photocatalysts are also prevalent for their elevated efficiency encompassing metal oxides/sulfides (TiO$_2$, CdS, ZnO, CeO$_2$, *etc.*),[9–12] polyoxometalates,[13] and organic metal complexes.[14,15] However, many of the aforementioned catalysts are either expensive or highly toxic, suffer from restricted visible-light absorption, demand high catalyst loading, exhibit inadequate efficiency, and fail to translate into large-scale applications. Furthermore, the separation of homogeneous catalysts from reaction systems for subsequent reuse poses a challenge. In this context, heterogeneous visible-light photocatalysts exhibit particular promise due to their exceptional recyclability and environmentally friendly characteristics.[16–18] Therefore, a viable

[a] *Key Laboratory of Polyoxometalate and Reticular Material Chemistry of Ministry Education, College of Chemistry, Northeast Normal University, Changchun 130024, P. R. China. E-mail: taox091@nenu.edu.cn*

[b] *College of Chemistry, Jilin University, Changchun 130012, P. R. China*

† Electronic supplementary information (ESI) available. See DOI: https://doi.org/10.1039/d4ey00071d

resolution to these challenges involves the exploration of efficient, durable, cost-effective, metal-free, and non-toxic heterogeneous photocatalysts that are both recyclable and reusable, aligning with the principles of "Green Chemistry".[19]

Porous aromatic frameworks (PAFs) possess high stability, expansive specific surface areas, substantial pore volumes, and robust modifiability.[20] Leveraging the diverse synthesis and functionalization options, it becomes feasible to tailor specific properties within PAF skeletons, presenting significant opportunities for applications in gas adsorption,[21] gas separation,[22] sensors,[23,24] and heterogeneous catalysis,[25] marking them as a noteworthy domain within the porous material family. The judicious selection of suitable building blocks and efficient coupling reaction types is imperative to obtain PAFs with precise structures and manageable properties.[20] PAFs exhibit elevated specific surface areas, extended π-conjugated skeletons, and layered stacking structures, establishing optimal conduits for carrier migration and charge separation. Remarkably, through meticulous framework design, adjustments to the optical band gaps, redox potentials, and light responsive ranges become attainable.[26] These unique features render PAFs a feasible and promising platform for constructing efficient porous organic photocatalysts.

In recent years, using donor (D)–acceptor (A) type photocatalysts, many exciting achievements in the field of photocatalytic energy conversion have been made.[27] As a prominent unit of aggregation-induced emission luminogens (AIEgens), tetraphenylethylene (TPE)[28] has been integrated into porous organic polymers,[29] demonstrating exemplary sensing performance. The propeller structure inherent in TPE introduces a pronounced noncoplanar packing effect through its side groups, significantly retarding intermolecular charge and energy transfer.[30] Because of its well conjugated structure and high π electron delocalization, it can be used as an ideal acceptor building block of photocatalysts.[27] Simultaneously, thiophene is one of the most studied heterocyclic compounds. Owing to the electron-donating nature of its sulfur atom, thiophene serves as a donor building block and imparts excellent conductivity and adjustable electron density.[31] Numerous studies have proved that thiophene units are active sites for the oxygen reduction reaction (ORR) in porous organic semiconductor induced photocatalysis.[32] Therefore, introducing thiophene and TPE units into the framework of PAFs in an alternating D–A fashion could effectively regulate the electron distribution that would favor photoinduced electron–hole pair separation. Meanwhile, the introduced thiophene units could potentially serve as active sites for the ORR, which would jointly improve their photocatalytic performance.

Based on these considerations, three TPE-containing D–A type PAFs (TPE-PAFs) are designed and synthesized by combining TPE and thiophene fragments with different electron donating abilities, including 2,2′-bithiophene (BTP), thieno[3,2b]thiophene (TBTP) and benzo[1,2-b:4,5-b′]dithiophene (BDTP). Their bandgaps, energy levels and photoelectric properties could be adjusted by changing the thiophene-derived linear linkers between TPE units. Under mild conditions, the obtained TPE-PAFs serve as efficient photocatalysts for the synthesis of benzimidazoles. The representative TPE-PAF photocatalyst could be recycled and reused for ten reaction cycles with unchanged photocatalytic performance. In addition, the heterogeneous catalytic reaction was monitored by using *in situ* IR spectra. Furthermore, their structure–property relationship is investigated, and the possible catalytic reaction mechanism is discussed from this perspective.

Results and discussion

Under solvothermal conditions, reaction of 1,1,2,2-tetrakis (4-bromophenyl)ethene (TPE-4Br) with BTP, TBTP and BDTP in the presence of $Pd_2(dba)_3$ through the direct arylation
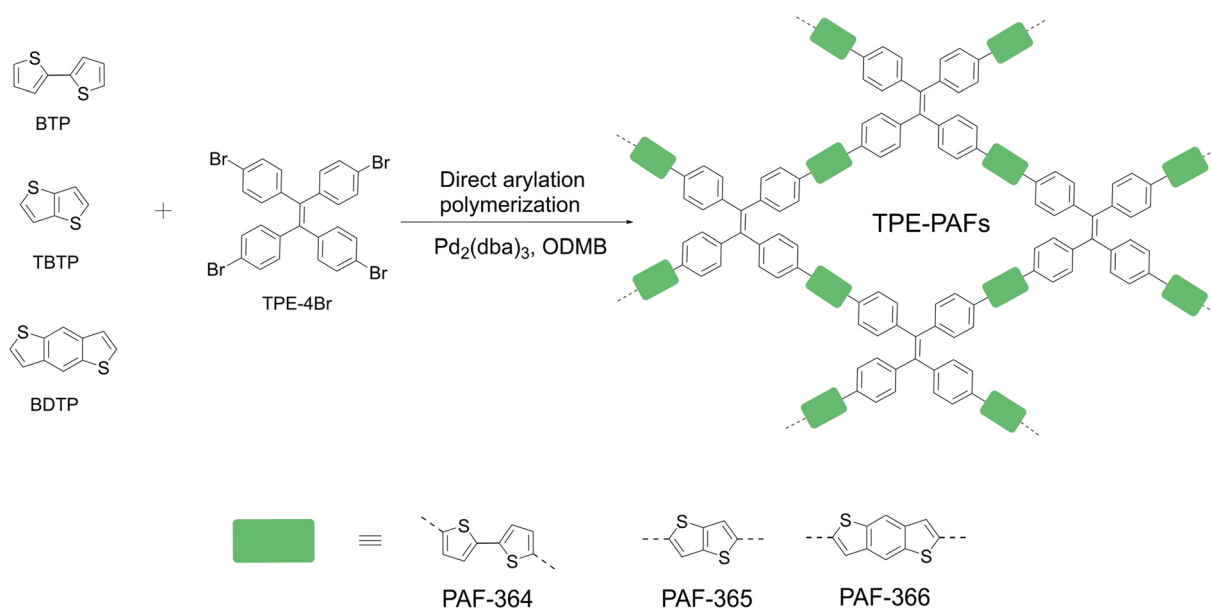
Scheme 1 Synthesis of PAF-364, PAF-365 and PAF-366.

polymerization reaction[33] gave the respective TPE-PAFs, named PAF-364, PAF-365 and PAF-366 in Scheme 1 (for details, see Scheme S1–S3, ESI†). The formation of three TPE-PAFs was evidenced by using various analytical techniques. Fourier transform infrared (FT-IR) spectroscopy was used to characterize TPE-4Br, PAF-364, PAF-365 and PAF-366 (Fig. 1a). The FT-IR spectra of TPE-PAFs clearly indicate the disappearance of the C–Br bonds (1066 cm^{-1}), thus demonstrating the success of the carbon–carbon coupling using a direct arylation polymerization method.[34] To further reveal the local structures of PAF-364, PAF-365 and PAF-366, we performed ^{13}C solid-state NMR studies (Fig. 1b). Signals ranging from 110.0 to 150 ppm are designated for sp^2-hybridised carbon atoms found in aryl spacers and thiophene moieties.[35] Especially, the signals at approximately 143.2 ppm are tentatively assigned to the ethylene carbon atoms.[36,37] Powder X-ray diffraction (PXRD) analysis was performed to confirm the long-range structure of TPE-PAFs. As shown in Fig. 1c, these TPE-PAFs are amorphous with no long-range crystallographic order and show a broad diffraction peak, which is consistent with the typical diffraction pattern of the PAF structure.[38] The Brunauer–Emmett–Teller (BET) surface areas of PAF-364, PAF-365 and PAF-366 were calculated as 152.7, 172.7 and 231.8 m^2 g^{-1}, respectively. As can be seen in Fig. 1d, classic type I nitrogen sorption isotherm plots indicate the micro-/mesoporous character of TPE-PAFs.[39,40] The pore size distributions of these TPE-PAFs were evaluated by using a nonlocal density functional theory (NLDFT) method. The dominant peaks were centered at 1.09–1.43 nm and 2–10 nm ranges for PAF-364, PAF-365 and PAF-366 (Fig. S1, ESI†). The survey of spectra obtained using X-ray photoelectron spectroscopy (XPS) (Fig. S2–S4, ESI†) indicate that TPE-PAFs were composed of carbon and sulfur elements. The C 1s XPS peaks were further analyzed to identify the presence of sp^2-C/sp^3-C, with a dominant peak observed at 284.8 eV.[41,42] Meanwhile, the XPS spectra of S 2p exhibit two distinct peaks at 164.2 eV and 165.3 eV, corresponding to –C–S–C– and –C═S– groups, respectively.[41–44] All these results indicate the successful synthesis of PAF-364, PAF-365 and PAF-366. Moreover, thermogravimetric analysis (TGA) indicates that these TPE-PAFs are thermally stable up to 300 °C under a N$_2$ atmosphere (Fig. S5, ESI†).

The morphology information was collected by using scanning electron microscopy (SEM) and transmission electron microscopy
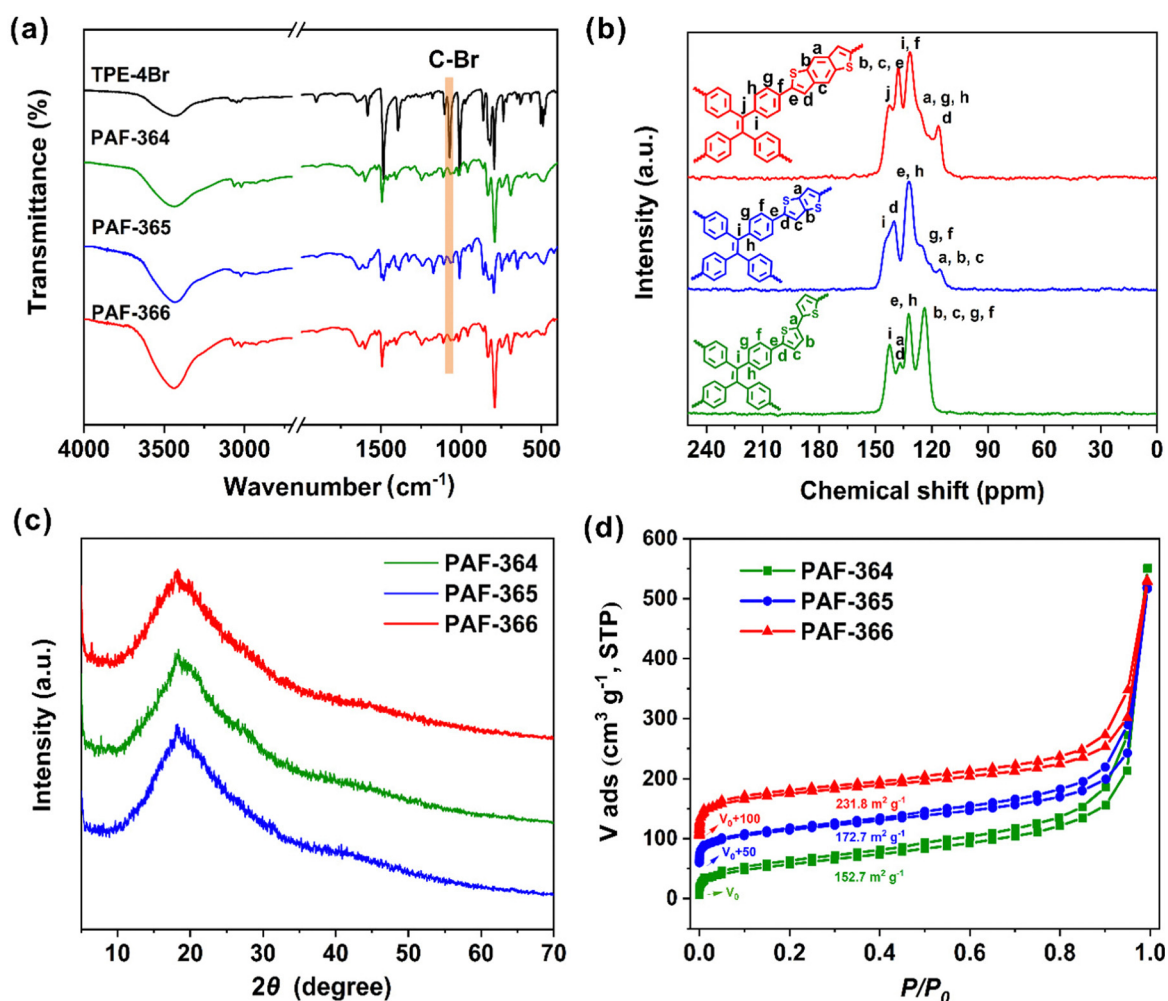

Fig. 1 Structural characterization of PAF-364, PAF-365 and PAF-366. (a) FT-IR spectra. (b) ^{13}C CP-MAS solid-state NMR spectra. (c) PXRD patterns. (d) N$_2$ adsorption/desorption isotherms at 77 K.

(TEM). The SEM images of the PAF-364, PAF-365 and PAF-366 are shown in Fig. 2a–c, indicating that they have the morphological structure of irregular nanoparticle interconnections. The TEM image in Fig. 2d demonstrates the presence of a hierarchical porous structure but no evidence of long-range ordering in PAF-366, which is consistent with the results obtained using PXRD. Furthermore, the TEM elemental mapping images in Fig. 2e and f reveal that the C and S elements are uniformly distributed on the skeleton of PAF-366.

To assess the photocatalytic performance, we investigated the optical and electrochemical properties of TPE-PAFs. Firstly, the TPE-PAFs were analyzed by UV-Vis diffuse reflectance spectroscopy. As shown in Fig. 3a, PAF-366 shows a wide visible light absorption peak from ultraviolet to 800 nm, with sharp absorption edges up to 600 nm. Compared with the visible light absorption peak of PAF-364 and PAF-365, PAF-366 has a better absorption capacity of visible light. Their optical band gaps are determined to be 2.19 eV for PAF-364, 2.29 eV for PAF-365 and 2.14 eV for PAF-366, which is calculated from the corresponding Tauc plots in Fig. 3b. In addition, density functional theory (DFT) was used to optimize the small molecule model compounds of the TPE-PAFs, which reveals that the PAF-366 has the smallest band gap (Fig. S6, ESI†) among TPE-PAFs. This is consistent with the experimental observations. To investigate the effect of the D–A system on the optical band gap structures, the conjugated microporous polymer TPE-CMP[45] composed of TPE only was synthesized, for a comparison, following the procedures described in the literature (Scheme S4 and Fig. S7,

S8, ESI†). The TPE-CMP displayed a narrow absorption band from ultraviolet region to 550 nm, with a sharp absorption edge up to 400 nm and the optical band gap was estimated to be about 2.65 eV. In comparison, red-shifted absorption bands and smaller optical band gaps for PAF-364, PAF-365 and PAF-366 are observed, which clearly demonstrates the effect of establishment of D–A systems on the optical properties of TPE-PAFs.[46] The construction of D–A system accurately adjusts the optical absorption range and the optical band gap. To conduct a more in-depth analysis on the relative positions of the valence band (VB) and conduction band (CB), the VB potentials were approximately determined by the VB-XPS spectra as 1.30 eV, 1.34 eV and 1.28 eV in Fig. 3c. Taking the VB potentials from the bandgap energy, the potential of the CB potentials ($E_g = E_{VB} - E_{CB}$) are calculated to be −0.89 eV, −0.95 eV and −0.86 eV in Fig. 3d. We can clearly observe that the energy band structures of these three PAFs can be easily adjusted by changing the thiophene units. The CB potentials of the TPE-PAFs were more negative than the potential of $O_2/O_2^{\bullet-}$ (−0.33 eV).[47,48] These data indicate that PAF-364, PAF-365 and PAF-366 could potentially serve as efficient photocatalysts for the oxygen reduction reaction (ORR).

It is well-known that the efficient generation, separation, and transport of photoinduced charge carriers in photocatalytic frameworks are crucial to improve the photocatalytic performance. Therefore, we further investigated the transient photocurrent response and conducted electrochemical impedance spectroscopy (EIS) of these TPE-PAFs. Upon visible light
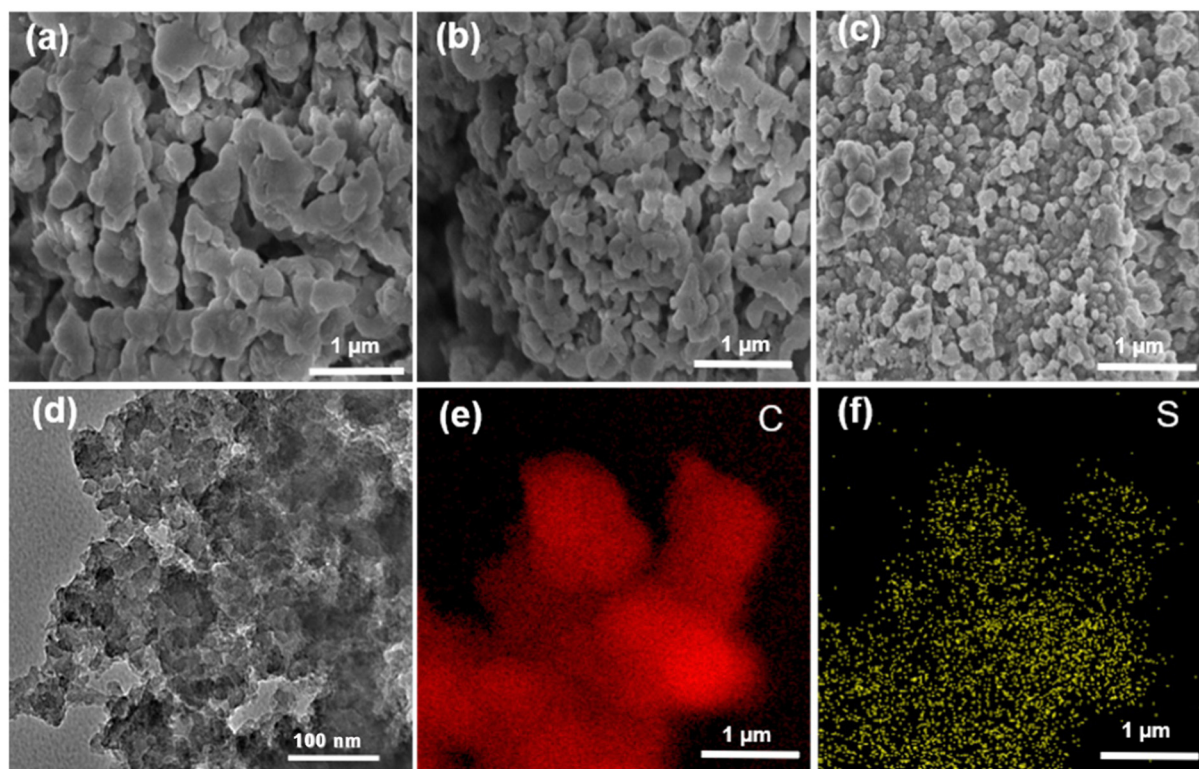

Fig. 2 SEM images of (a) PAF-364, (b) PAF-365, (c) PAF-366. (d)–(f) TEM image and TEM elemental mapping of PAF-366.
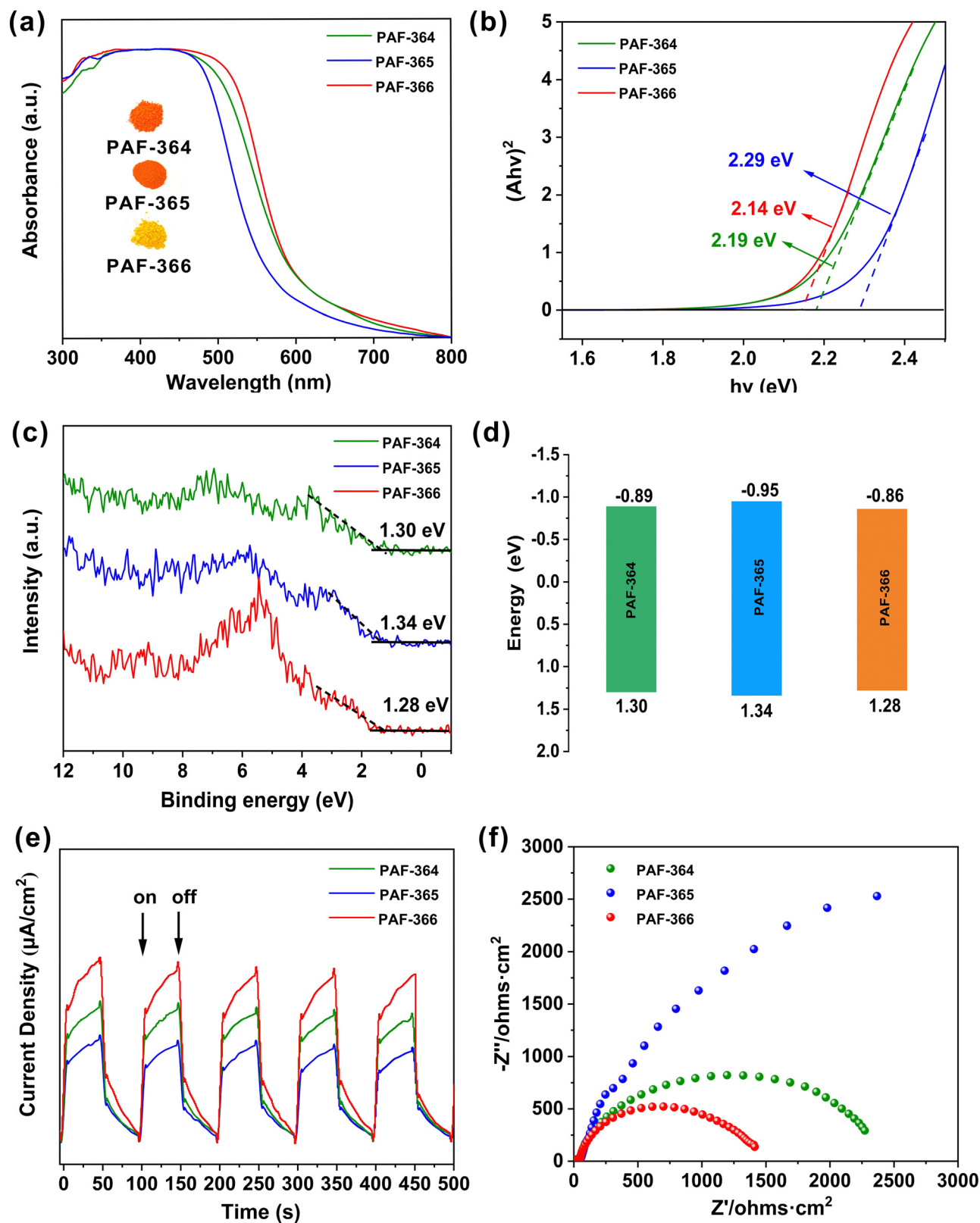
Fig. 3 (a) Solid-state absorption profiles. (b) Tauc plots. (c) VB-XPS spectra. (d) Schematic diagram of the energy band structure. (e) Transient photocurrent responses under light irradiation. (f) The EIS Nyquist plots of PAF-364, PAF-365 and PAF-366.

irradiation, TPE-PAFs exhibit a fast photocurrent response, accompanied by a considerable number of intermittent switching

illumination repetition cycles (Fig. 3e). This clearly demonstrates the photoinduced carrier transfer in TPE-PAFs.[45,48] Among them,
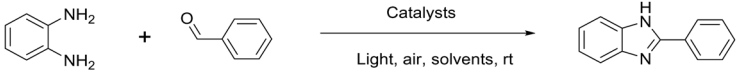
PAF-366 shows the highest photocurrent response value, indicating a higher charge separation efficiency and more available surface carriers in the photocatalytic process. In addition, the EIS Nyquist plot of PAF-366 shows the smallest arc radius among these three PAFs (Fig. 3f), indicating that the charge transfer barrier in PAF-366 decreases with increasing charge density.[46,49] These observations imply that PAF-366 may serve as a more efficient photocatalyst in comparison with PAF-364 and PAF-365, which is consistent with the following photocatalytic experiments.

Benzimidazole derivatives are important intermediates in organic synthesis, which also widely exist in the molecular skeletal structure of biologically active molecules, such as antihypertensive, anticancer, antiviral, psychotropic, antifungal and anti-arrhythmic drugs.[50] To evaluate the practical utility of the TPE-PAFs as photocatalysts, their photocatalytic performance for the synthesis of benzimidazoles was investigated. Reaction of benzaldehyde and *o*-phenylenediamine to produce benzimidazole was selected as the model reaction to screen the optimal reaction conditions in Table 1. Under similar conditions, PAF-366 exhibits superior photocatalytic efficiency among these TPE-PAFs, which achieved a higher yield (90%) of 2-phenyl-1*H*-benzo[*d*]imidazole (Table 1, 1–3). It is noteworthy that these three TPE-PAFs all achieve higher yield for the benzimidazole formation reaction in comparison with the reported TPE-CMP photocatalyst (Table 1, 4), which indicates that the construction of D–A system is beneficial to the improvement of photocatalytic efficiency. Subsequently, we explored the effect of the catalyst loading on the yield. The optimal catalyst loading of PAF-366 is 2 mg (5.6 mol%), which gives the optimal yield (99%) of 2-phenyl-1*H*-benzo[*d*]imidazole product under similar reaction conditions. The addition of a large amount of insoluble photocatalyst may cause light scattering, which could reduce the amounts of photons obtained per unit weight of the catalyst (Table 1, 3 and 5–7). Moreover, the reaction solvent is also found to be crucial for the catalytic

efficiency of this reaction. When the protic solvent ethanol (C_2H_5OH) and methanol (CH_3OH) are used, the reaction yields of 99% and 97% are achieved, respectively (Table 1, entries 6 and 8). Therefore, we use C_2H_5OH as the reaction solvent. Under similar conditions, much lower yields ranging from 0% to 53% in aprotic solvents such as 1,4-dioxane, tetrahydrofuran (THF), toluene, acetonitrile (CH_3CN), *N*,*N*-dimethylformamide (DMF), acetone and dichloromethane (CH_2Cl_2) are obtained for the PAF-366 catalysed photosynthesis of 2-phenyl-1*H*-benzo[*d*]imidazole (Table 1, entries 9–15). Similarly, PAF-364 and PAF-365 show lower photocatalytic activities in aprotic solvents than PAF-366 for this reaction (Table S1 (ESI†), entries 1–14).

Furthermore, a series of control experiments were carried out to investigate the reaction mechanism of TPE-PAF catalyzed photosynthesis of benzimidazoles (Fig. 4a). The presence of photocatalyst, light irradiation and air are indispensable for the model reaction. To verify the generation of reactive oxygen species in this photocatalytic process, 2,2,6,6-tetra methylpiperidine-1-oxyl (TEMPO) or *p*-benzoquinone (*p*-BQ) was added to the reaction mixture as a free radical or superoxide radical anion scavenger, respectively, which resulted in the decreased yields. This indicates that the superoxide radical anion is indeed the key reactive oxygen species for this reaction. However, the addition of sodium azide (NaN_3) ($^1O_2$ scavenger) did not have an adverse effect on the yield. On this basis, the major reactive oxygen species here should be $O_2^{•-}$ rather than $^1O_2$. Furthermore, the model photocatalytic reaction is severely suppressed when photoexcited electron (e^-) scavenger $CuCl_2$ or photogenerated hole (h^+) scavenger KI is added. This implies that h^+ and e^- are both crucial for this photocatalytic reaction. Furthermore, the PAF-366 promoted electron transfer from *N*,*N*,*N'*,*N'*-tetramethyl-*p*-phenylenediamine (TMPD) to molecular oxygen upon light irradiation was monitored by the obvious color change, due to the possible formation of a nitrogen radical cation and superoxide anion (Fig. 4b).[46] To characterize the *in situ* generated reactive oxygen species in

Table 1 Optimization of the reaction conditions[a]

Entry	Catalyst	Amount[b] (mg, mol%)	Solvent	Yield[c] (%)
1	PAF-364	3, 9.0	C_2H_5OH	74
2	PAF-365	3, 9.8	C_2H_5OH	63
3	PAF-366	3, 8.4	C_2H_5OH	90
4[d]	TPE-CMP	3, 18.0	C_2H_5OH	48
5	PAF-366	1, 2.8	C_2H_5OH	93
6	PAF-366	2, 5.6	C_2H_5OH	99
7	PAF-366	4, 11.2	C_2H_5OH	88
8	PAF-366	2, 5.6	CH_3OH	97
9	PAF-366	2, 5.6	1,4-Dioxane	53
10	PAF-366	2, 5.6	THF	Trace
11	PAF-366	2, 5.6	Toluene	13
12	PAF-366	2, 5.6	CH_3CN	32
13	PAF-366	2, 5.6	DMF	Trace
14	PAF-366	2, 5.6	Acetone	6
15	PAF-366	2, 5.6	CH_2Cl_2	24

[a] *o*-Phenylenediamine (0.2 mmol), benzaldehyde (0.2 mmol), solvent (4 mL), air, 460 nm blue LED lamp (24 W, 0.08 W cm^{-2}), 298 K, 3 h. [b] The molar ratio of the repeating units of the catalysts *versus* substrates. [c] Isolated yields. [d] TPE-CMP as the heterogeneous catalyst.
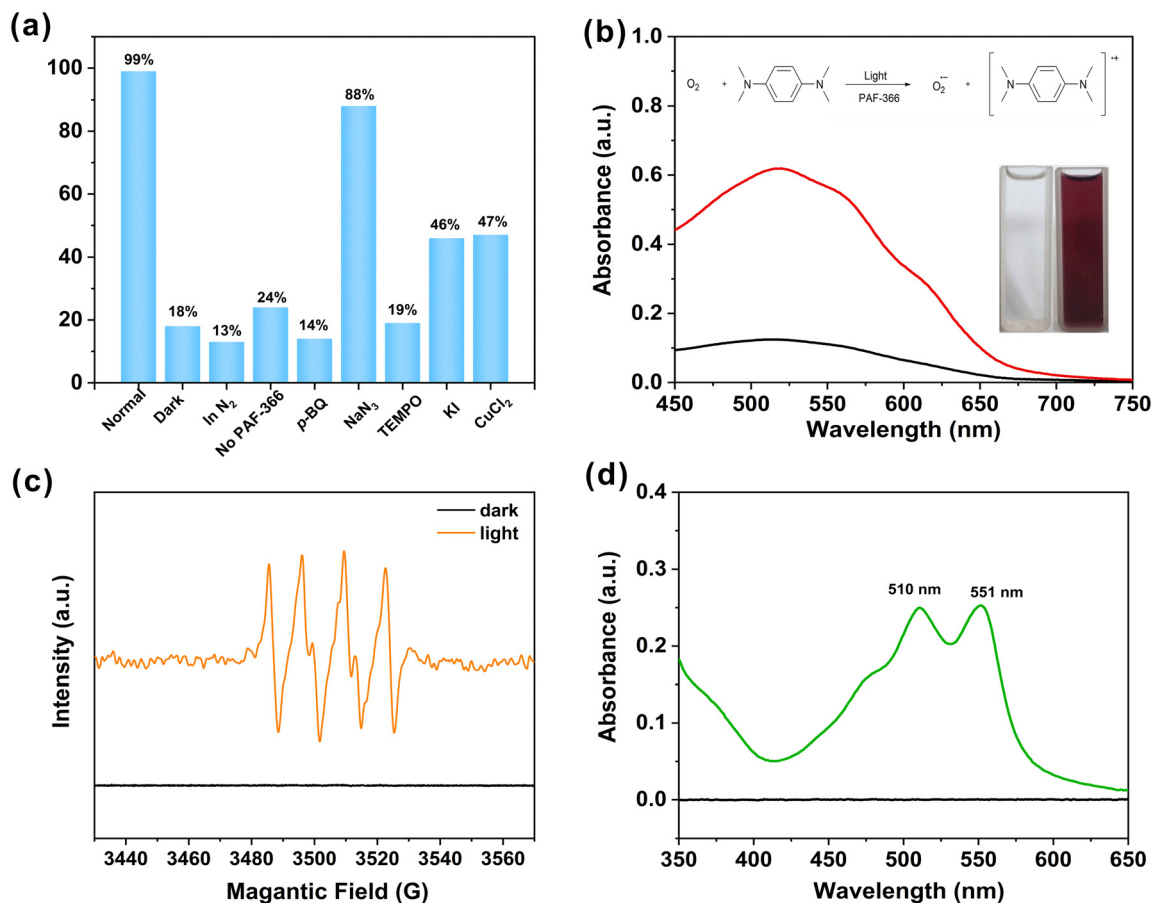
Fig. 4 (a) Control experiments by PAF-366 under different conditions (o-phenylenediamine (0.2 mmol), benzaldehyde (0.2 mmol), C_2H_5OH (4 mL), 298 K, 3 h. p-BQ as the superoxide scavenger; NaN₃ as the singlet oxygen scavenger; TEMPO as the radical scavenger; KI as the hole scavenger; CuCl₂ as the electron scavenger). (b) UV-vis absorption spectra and photograph of the cationic radical of TMPD generated by PAF-366 in the presence of light and air. (c) ESR spectra of PAF-366 (2.0 mg mL^{-1}) and DMPO (0.1 M) in methanol under dark and light illumination. (d) UV-vis absorption spectra of the reaction system after adding DPD and POD for H_2O_2 determination.

the photocatalytic reaction, the spin-trapping electron–spin reso-nance (ESR) experiments were performed. 5,5-Dimethyl-1-pyrro-line-N-oxide (DMPO) and 2,2,6,6-tetramethyl-4-piperidone hydro-chloride (TEMP) are used as spin-trapping agents to detect reactive oxygen species $O_2^{\bullet-}$ and $^1O_2$, respectively. A typical signal pattern of DMPO-$O_2^{\bullet-}$ in the spin-trapping ESR spectrum is observed (Fig. 4c), which proved that $O_2^{\bullet-}$ is generated easily within the PAF-366 induced photocatalytic system. In contrast, no signal is observed in the TEMP-$^1O_2$ spin-trapping ESR experiment (Fig. S9, ESI†), indicating that $^1O_2$ is not the key reactive oxygen species in the PAF-366 induced photocatalytic system. It should be noted that only a minimal quantity of 2-methylbenzimidazole was detected in the catalytic reaction mixture (Fig. S10, ESI†), which was likely produced by the reaction of o-phenylenediamine with a small amount of acetaldehyde that was generated from the oxidation of ethanol. The formation of H_2O_2, one of the postu-lated intermediates in the aerobic oxidation reactions is also detected by using the catalyzed oxidation of N,N-diethyl-1,4-phenylenediammonium sulphate (DPD) by horseradish peroxi-dase (POD), due to which two absorption peaks at 510 and 551 nm (Fig. 4d) can be seen.

Based on the above observations, a possible reaction mecha-nism is proposed in Fig. 5. Under visible light irradiation, the electron (e^-) and hole (h^+) separation on the surface of PAF-366 photocatalyst should occur. On the other hand, the condensa-tion between o-phenylenediamine and benzaldehyde could form imine-containing intermediate I ($E(I/I^{\bullet+})$ = 0.45 V), which could be subsequently oxidized by the photogenerated h^+ to give intermediate $I^{\bullet+}$. The proton in intermediate $I^{\bullet+}$ should be very acidic and tends to be abstracted by a strong base to form intermediate II, which then undergoes a cyclization and a reduction by photoexcited e^- to generate intermediate III. Subsequent deprotonation by bases gives intermediate IV, which could further undergo oxidation by h^+ through a single electron transfer process that ultimately yields a nitrogen-centered radical cation intermediate V. Deprotonation of the intermediate V by in situ generated $O_2^{\bullet-}$ followed by hydrogen atom abstraction gives the target product 2-phenyl-1H-benzo-[d]imidazole and H_2O_2. This is consistent with the reaction mechanism described in the literature.[37,44,48–52]

To gain an insight into the evolution of the photosynthetic reaction of benzimidazoles, the three-dimensional FT-IR (3D-
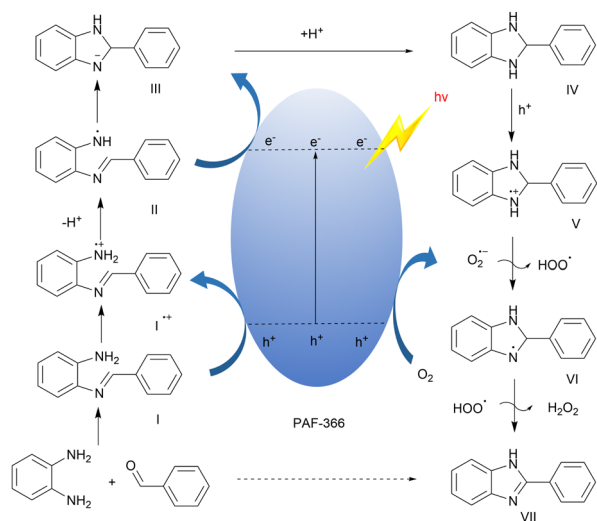
Fig. 5 Possible photosynthetic reaction mechanism of 2-phenyl-1*H*-benzo[*d*]imidazole catalyzed by PAF-366 under visible light irradiation.

FTIR) measurements were performed, and the profiles are also presented in Fig. 6. In the 3D-FTIR spectra of the PAF-366 catalyzed photoreaction mixture, the two bands centered at 1205 cm^{-1} and 1707 cm^{-1} correspond to the C–N stretching vibration of *o*-phenylenediamine and the C=O stretching vibration of benzaldehyde, respectively.[53,54] These characteristic peaks of the two reactants gradually decreased with prolonging reaction time. Meanwhile, two characteristic peaks of 1540 cm^{-1} and 1398 cm^{-1} attributed to the C=N stretching vibration and C–N stretching vibration of benzimidazole,[55] respectively, are observed, whose intensities increase rapidly with extension of the reaction time. This clearly shows the process of the formation of benzimidazole product with consumption of two starting materials *o*-phenylenediamine and benzaldehyde. This process can also be monitored *via* the nuclear magnetism (NMR) experiment. These observations prove that PAF-366 can serve as an efficient photocatalyst for the synthesis of benzimidazoles.

With the optimal reaction conditions available, we investigated the substrate scope of PAF-366 catalyzed photosynthesis of benzimidazole. It was found that aldehydes with different substituents such as aromatic groups, alky groups and heterocycles are suitable for this photocatalytic reaction. Using non-substituted benzaldehyde as the starting material, this reaction
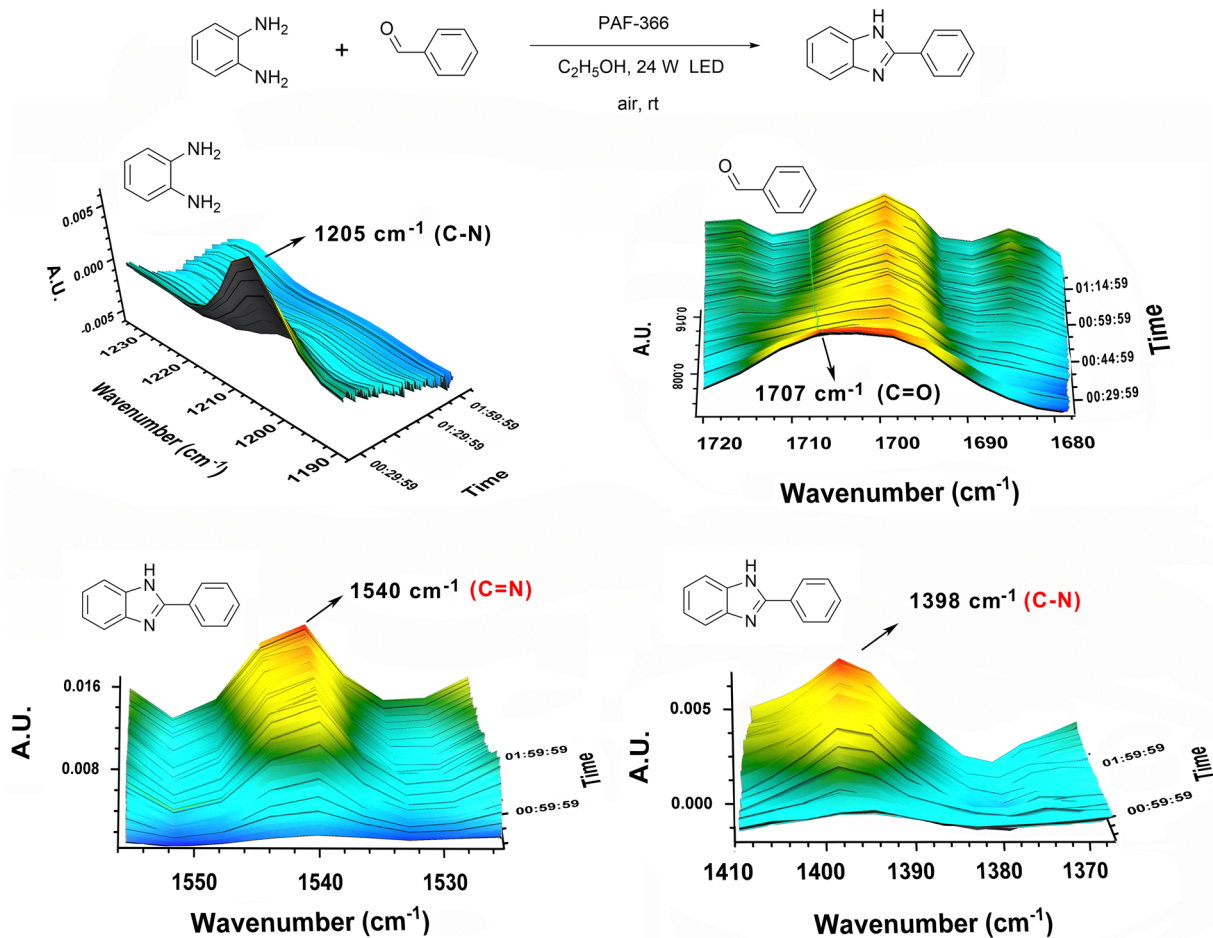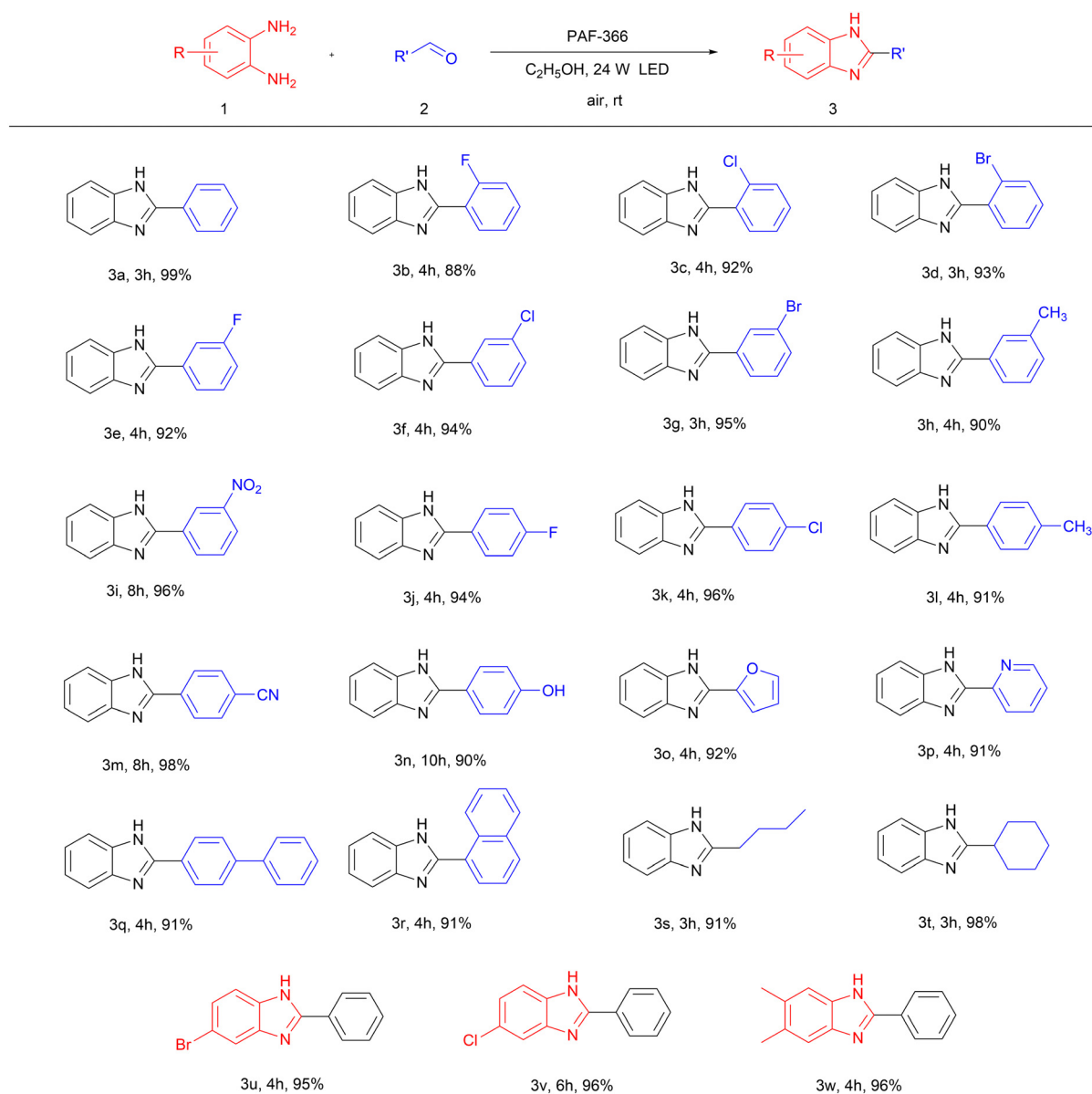

Fig. 6 *In situ* IR spectra of reaction mixture of benzimidazole photosynthesis. Reaction conditions: *o*-phenylenediamine (0.2 mmol), benzaldehyde (0.2 mmol), PAF-366 (2 mg, 5.6 mol%), C$_2$H$_5$OH (4.0 mL), air, 460 nm blue LED lamp (24 W, 0.08 W cm^{-2}), 298 K, 2 h.

proceeds within 3 h to give the benzimidazole product in 99% yield (Table 2 **3a**). The *ortho*-substituted benzaldehydes afford the benzimidazole product in slightly lower yields (88∼93%) (Table 2 **3b–3d**), while the *meta*- or *para*-substituted benzaldehydes could slightly increase the yields (90∼98%) (Table 2 **3e–3n**). In particular, the photocatalytic reactions with the –NO$_2$, –CN and –OH substituted benzaldehydes as starting materials need a longer reaction time (Table 2 **3i, 3m** and **3n**). It is also found that the same substituents at the *meta*- or *para*-positions show higher reactivity than that at the *ortho*-position of benzaldehydes, probably due to the steric hindrance effect (Table 2 **3b, 3e, 3j**). It is worth mentioning that our photocatalytic system is compatible to heteroaromatic aldehydes, as evidenced by the moderate yields obtained from furan-2-carbaldehyde or picolinaldehyde substrates (Table 2 **3o** and **3p**). When *p*-phenylbenzaldehyde and 1-naphthaldehyde are used as reaction substrates, the target products can also be obtained in 91% yield (Table 2 **3q** and **3r**). It should be noted that this system can also be utilized for the production of benzimidazoles featuring an alkyl or cycloalkyl moiety at the 2-position. (Table 2 **3s** and **3t**). Meanwhile, the substituted *o*-phenylenediamines, also found to be compatible for this photocatalytic reaction, together with benzaldehyde as starting materials afford a high yield (95∼96%) of substituted benzimidazole products (Table 2 **3u–3w**). Additionally, a relatively large-scale photocatalytic synthesis of **3a** has a yield of 93% (902.8 mg) (Fig. S11, ESI†). In

Table 2 Substrate scope of photosynthesis of benzimidazoles catalysed by PAF-366

3a, 3h, 99%   3b, 4h, 88%   3c, 4h, 92%   3d, 3h, 93%

3e, 4h, 92%   3f, 4h, 94%   3g, 3h, 95%   3h, 4h, 90%

3i, 8h, 96%   3j, 4h, 94%   3k, 4h, 96%   3l, 4h, 91%

3m, 8h, 98%   3n, 10h, 90%   3o, 4h, 92%   3p, 4h, 91%

3q, 4h, 91%   3r, 4h, 91%   3s, 3h, 91%   3t, 3h, 98%

3u, 4h, 95%   3v, 6h, 96%   3w, 4h, 96%

Conditions: anilines (0.2 mmol), aldehydes (0.2 mmol), PAF-366 (2 mg, 5.6 mol%), C$_2$H$_5$OH (4.0 mL), air, 298 K, 460 nm blue LED lamp (24 W, 0.08 W cm^{-2}), yields of isolated products.

heterogeneous catalytic systems, the recyclability of catalysts is a main concern. Therefore, we explored the recyclability and reusability of the PAF-366 photocatalyst for the synthesis of benzimidazole using o-phenylenediamine and benzaldehyde as starting materials (Fig. S12a, ESI†). The PAF-366 photocatalyst could be recycled by simple washing with THF and C_2H_5OH and reused for the next photocatalytic cycle. It was found that the photocatalytic activity of PAF-366 remains, and it could be reused even after ten reaction cycles. More importantly, the recycled PAF-366 retains its original chemical structure (Fig. S12b–d and S13, ESI†), mainly due to its stability, indicating that PAF-366 is potentially applicable for industrial production.

Conclusions

In summary, we have successfully developed three TPE-containing D–A type PAF photocatalysts PAF-364, PAF-365 and PAF-366 using TPE as the acceptor unit and different thiophenes as donor units. The range of optical absorption, the band structures, and optoelectronic properties of these photocatalyst are precisely tuned based on their structural variation. It was found that PAF-366 exhibits superior photocatalytic activity for the synthesis of benzimidazole derivatives with extensive substrate compatibility and excellent recyclability. Moreover, this photocatalytic reaction system aligns with the principles of green chemistry by eliminating the need for oxidants or metals. Overall, this study presents a viable strategy for constructing PAF-based photocatalysts, which further broadens the application of PAF materials in photocatalytic technology.

Author contributions

X. T.: conceptualization, date curation, formal analysis, funding acquisition, investigation, methodology, writing – review & editing. H. W.: investigation, methodology, date curation, formal analysis, methodology, writing – original draft. X. X.: investigation, methodology, formal analysis. L. C., Z. Z. and J. L.: investigation, methodology. X. L.: investigation, methodology, conceptualization. G. Z.: investigation, methodology, conceptualization.

Conflicts of interest

There are no conflicts to declare.

Acknowledgements

Notes and references

1 C. Li, N. Mizuno, K. Murata, K. Ishii, T. Suenobu, K. Yamaguchi and K. Suzuki, *Green Chem.*, 2020, **22**, 3896–3905.

2 S. Kato, J. Jung, T. Suenobu and S. Fukuzumi, *Energy Environ. Sci.*, 2013, **6**, 3756–3764.

3 Y. M. Pang, P. F. Li, X. B. Ma, L. Sun, Y. C. Liu, D. Qu, L. An and Z. C. Sun, *EES. Catal.*, 2023, **1**, 810–831.

4 C. J. Wu, X. Y. Li, T. R. Li, M. Z. Shao, L. J. Niu, X. F. Lu, J. L. Kan, Y. Geng and Y. B. Dong, *J. Am. Chem. Soc.*, 2022, **144**, 18750–18755.

5 N. Y. Huang, Y. T. Zheng, D. Chen, Z. Y. Chen, C. Z. Huang and Q. Xu, *Chem. Soc. Rev.*, 2023, **52**, 7949–8004.

6 S. H. Wei, L. Wang, J. Y. Yue, R. Wu, Z. B. Fang and Y. X. Xu, *J. Mater. Chem. A*, 2023, **11**, 23720–23741.

7 M. Gryszel, R. Rybakiewicz and E. D. Głowacki, *Adv. Sustainable Syst.*, 2019, **3**, 1900027.

8 S. Sharma and A. Sharma, *Org. Biomol. Chem.*, 2019, **17**, 4384–4405.

9 M. D. Hernandez-Alonso, F. Fresno, S. Suarez and J. M. Coronado, *Energy Environ. Sci.*, 2009, **2**, 1231–1257.

10 D. P. Benu, A. Andriani, N. Silmi, F. V. Steky, F. Failamani, B. Yuliarto, R. R. Mukti and V. Suendo, *New J. Chem.*, 2023, **47**, 428–442.

11 Y. P. Xie, Z. B. Yu, G. Liu, X. L. Ma and H. M. Cheng, *Energy Environ. Sci.*, 2014, **7**, 1895–1901.

12 S. Yang, W. Zhang, G. Pan, J. Chen, J. Deng, K. Chen, X. Xie, D. Han, M. Dai and L. Niu, *Angew. Chem., Int. Ed.*, 2023, **62**, e202312076.

13 H.-J. Lee and E. S. Cho, *ACS Sustainable Chem. Eng.*, 2023, **11**, 7624–7632.

14 H. Zheng, Y. Hou, S. Li, J. Ma, J. Nan and T. Li, *Chin. Chem. Lett.*, 2022, **33**, 5013–5022.

15 H. Zhao, Q. Xia, H. Xing, D. Chen and H. Wang, *ACS Sustainable Chem. Eng.*, 2017, **5**, 4449–4456.

16 X. Lang, X. Chen and J. Zhao, *Chem. Soc. Rev.*, 2014, **43**, 473–486.

17 Y.-J. Quan, W.-J. Shi, Y. Song, X.-M. Jiang, C. Wang and W.-B. Lin, *J. Am. Chem. Soc.*, 2021, **143**, 3075–3080.

18 Z. W. Zhang, J. Jia, Y. F. Zhi, S. Ma and X. M. Liu, *Chem. Soc. Rev.*, 2022, **51**, 2444–2490.

19 P. Anastas and N. Eghbali, *Chem. Soc. Rev.*, 2010, **39**, 301–312.

20 Y. Tian and G. Zhu, *Chem. Rev.*, 2020, **120**, 8934–8986.

21 T. Ben, H. Ren, S. Ma, D. Cao, J. Lan, X. Jing, W. Wang, J. Xu, F. Deng, J. M. Simmons, S. Qiu and G. Zhu, *Angew. Chem., Int. Ed.*, 2009, **48**, 9457–9460.

22 P. Zhang, X. Zou, J. Song, Y. Tian, Y. Zhu, G. Yu, Y. Yuan and G. Zhu, *Adv. Mater.*, 2020, **32**, 1907449–1907455.

23 T. Ma, X. Zhao, Y. Matsuo, J. Song, R. Zhao, M. Faheem, M. Chen, Y. Zhang, Y. Tian and G. Zhu, *J. Mater. Chem. C*, 2019, **7**, 2327–2332.

24 Y. Yuan, H. Ren, F. Sun, X. Jing, K. Cai, X. Zhao, Y. Wang, Y. Wei and G. Zhu, *J. Phys. Chem. C*, 2012, **116**, 26431–26435.

25 A. Dai, S. Li, T. Wang, Y. Yang, Y. Tian, X. Jing and G. Zhu, *Chin. Chem. Lett.*, 2023, **34**, 107559.

26 N. Yin, W. Chen, Y. Yang, Z. Tang, P. Li, X. Zhang, L. Tang, T. Wang, Y. Wang, Y. Zhou and Z. Zou, *Chin. J. Catal.*, 2023, **51**, 168–179.

27 L. Wang, L. Liu, Y. Li, Y. Xu, W. Nie, Z. Cheng, Q. Zhou, L. Wang and Z. Fan, *Adv. Energy Mater.*, 2024, **14**, 2303346.

28 Y. Liu, C. Deng, L. Tang, A. Qin, R. Hu, J. Z. Sun and B. Z. Tang, *J. Am. Chem. Soc.*, 2011, **133**, 660–663.

29 T. H. Weng, M. G. Mohamed, S. U. Sharma, S. V. Chaganti, M. M. Samy, J. T. Lee and S. W. Kuo, *ACS Appl. Energy Mater.*, 2022, **5**, 14239–14249.

30 X. He, H. Bi and P. F. Wei, *J. Mater. Chem. C*, 2023, **11**, 3675–3691.

31 X. Qin, X. Wu, L. Tang, X. Chen, M. Li, Y. Mou, B. Su, S. Wang, C. Feng, J. Liu, X. Yuan, Y. Zhao and H. Wang, *Nat. Commun.*, 2023, **14**, 5238.

32 D. Li, C. Li, L. Zhang, H. Li, L. Zhu, D. Yang, Q. Fang, S. Qiu and X. Yao, *J. Am. Chem. Soc.*, 2020, **142**, 8104–8108.

33 H. Bohra and M. Wang, *ACS Appl. Polym. Mater.*, 2019, **1**, 1697–1706.

34 Q. Zhuang, H. Chen, C. Zhang, S. Cheng, W. Dong and A. Xie, *J. Hazard. Mater.*, 2022, **434**, 128938.

35 Y. S. Kochergin, D. Schwarz, A. Acharjya, A. Ichangi, R. Kulkarni, P. Eliasova, J. Vacek, J. Schmidt, A. Thomas and M. J. Bojdys, *Angew. Chem., Int. Ed.*, 2018, **57**, 14188–14192.

36 Y. Zheng, H. Wang and J. Jiang, *Dyes Pigm.*, 2020, **173**, 107929.

37 W. An, S. Zheng, Y. Du, S. Ding, Z. Li, S. Jiang, Y. Qin, X. Liu, P. Wei, Z. Cao, M. Song and Z. Pan, *Catal. Sci. Technol.*, 2020, **10**, 5171–5180.

38 L. Wang, J. Jia, M. Faheem, Y. Tian and G. Zhu, *J. Ind. Eng. Chem.*, 2018, **67**, 373–379.

39 Z. Yu, L. Huang, Z. Sun, F. Cai, M. Liang and Z. Luo, *J. Power Sources*, 2022, **550**, 232149.

40 M. G. Kotp, S. U. Sharma, J.-T. Lee, A. F. M. EL-Mahdy and S.-W. Kuo, *J. Taiwan Inst. Chem. Eng.*, 2022, **134**, 104310.

41 X. Li, H. Xiong and Q. Jia, *ACS Appl. Mater. Interfaces*, 2019, **11**, 46205–46211.

42 T. Wu, M. Jing, Y. Tian, L. Yang, J. Hu, X. Cao, G. Zou, H. Hou and X. Ji, *Adv. Funct. Mater.*, 2019, **29**, 1900941.

43 S. Li, L. Dai, L. Li, A. W. Dong, J. N. Li, X. J. Meng, B. Wang and P. F. Li, *J. Mater. Chem. A*, 2022, **10**, 13325–13332.

44 B. Luo, Y. Chen, Y. Zhang and J. Huo, *J. Catal.*, 2021, **402**, 52–60.

45 Y. Xu, L. Chen, Z. Guo, A. Nagai and D. Jiang, *J. Am. Chem. Soc.*, 2011, **133**, 17622–17625.

46 Z. Li, S. Han, C. Li, P. Shao, H. Xia, H. Li, X. Chen, X. Feng and X. Liu, *J. Mater. Chem. A*, 2020, **8**, 8706–8715.

47 C. Chu, Y. C. Qin, C. L. Ni and J. P. Zou, *Chin. Chem. Lett.*, 2022, **33**, 2736–2740.

48 S. Han, Z. Li, S. Ma, Y. Zhi, H. Xia, X. Chen and X. Liu, *J. Mater. Chem. A*, 2021, **9**, 3333–3340.

49 W.-K. An, S.-J. Zheng, H.-X. Zhang, T.-T. Shang, H.-R. Wang, X.-J. Xu, Q. Jin, Y. Qin, Y. Ren, S. Jiang, C.-L. Xu, M.-S. Hou and Z. Pan, *Green Chem.*, 2021, **23**, 1292–1299.

50 Z. Li, H. Song, R. Guo, M. Zuo, C. Hou, S. Sun, X. He, Z. Sun and W. Chu, *Green Chem.*, 2019, **21**, 3602–3605.

51 C. Su, M. Acik, K. Takai, J. Lu, S. J. Hao, Y. Zheng, P. Wu, Q. Bao, T. Enoki, Y. J. Chabal and K. P. Loh, *Nat. Commun.*, 2012, **3**, 1298.

52 M. Li, S. Mei, Y. Zheng, L. Wang and L. Ye, *Chem. Commun.*, 2023, **59**, 13478–13481.

53 E. Kose, M. Karabacak, F. Bardak and A. Atac, *J. Mol. Struct.*, 2016, **1123**, 284–299.

54 A. Acharjya, P. Pachfule, J. Roeser, F. J. Schmitt and A. Thomas, *Angew. Chem., Int. Ed.*, 2019, **58**, 14865–14870.

55 H. Saral, Ö. Özdamar, I. Ucar, Y. Bekdemir and M. Aygun, *J. Mol. Struct.*, 2016, **1103**, 9–19.